Self-supervised Multiplex Consensus Mamba for General Image Fusion

Yingying Wang[1], Rongjin Zhuang[1], Hui Zheng[1], Xuanhua He[2], Ke Cao[3],
Xiaotong Tu[1*], Xinghao Ding[1]

[1] Key Laboratory of Multimedia Trusted Perception and Efficient Computing,
Ministry of Education of China, Xiamen University, China
[2]The Hong Kong University of Science and Technology
[3]University of Science and Technology of China
wangyingying7@stu.xmu.edu.cn, {xttu, dxh}@xmu.edu.cn

Abstract

Image fusion integrates complementary information from different modalities to generate high-quality fused images, thereby enhancing downstream tasks such as object detection and semantic segmentation. Unlike task-specific techniques that primarily focus on consolidating inter-modal information, general image fusion needs to address a wide range of tasks while improving performance without increasing complexity. To achieve this, we propose SMC-Mamba, a Self-supervised Multiplex Consensus Mamba framework for general image fusion. Specifically, the Modality-Agnostic Feature Enhancement (MAFE) module preserves fine details through adaptive gating and enhances global representations via spatial-channel and frequency-rotational scanning. The Multiplex Consensus Cross-modal Mamba (MCCM) module enables dynamic collaboration among experts, reaching a consensus to efficiently integrate complementary information from multiple modalities. The cross-modal scanning within MCCM further strengthens feature interactions across modalities, facilitating seamless integration of critical information from both sources. Additionally, we introduce a Bi-level Self-supervised Contrastive Learning Loss (BSCL), which preserves high-frequency information without increasing computational overhead while simultaneously boosting performance in downstream tasks. Extensive experiments demonstrate that our approach outperforms state-of-the-art (SOTA) image fusion algorithms in tasks such as infrared-visible, medical, multi-focus, and multi-exposure fusion, as well as downstream visual tasks.

Introduction

Due to hardware limitations, single sensors often fail to capture the full complexity of real-world scenes. Image fusion addresses this by integrating complementary information. This field can be categorized into multi-modal image fusion (MMIF), including infrared-visible (IVIF) and medical image (MDIF) fusion, and digital photographic image fusion (DPIF), which covers multi-focus (MFIF) and multi-exposure (MEIF) image fusion.

In recent years, deep learning has become the dominant approach for image fusion (Liu et al. 2024a,b; Li et al. 2025b; Zhang et al. 2025), mainly leveraging CNNs (Wang

et al. 2023) and Transformers (Li et al. 2025a). CNNs are effective at capturing local features but struggle with long-range dependencies due to limited receptive fields. Transformers address this with global self-attention, but suffer from high computational costs that scale quadratically with input size. State Space Models (SSMs), particularly Mamba (Gu and Dao 2023), offer a compelling alternative. Mamba enables global context modeling with linear complexity, overcoming the limitations of both CNNs and Transformers. These strengths inspire us to explore Mamba for efficient and scalable image fusion.

Existing image fusion methods predominantly concentrate on single-task designs, limiting their generalization across diverse tasks. Each fusion task—IVIF, MDIF, MFIF, and MEIF—has distinct goals, yet all aim to preserve high-frequency textures and structural details. A dynamic architecture that adapts to varying modalities can better handle these differences. Mixture of Experts (MoE) (Jordan and Jacobs 1994) offers a promising solution by leveraging expert modules to address diverse objectives, improving fusion quality and supporting downstream vision tasks.

However, existing deep learning methods often emphasize low-frequency content, struggling to accurately capture fine-grained high-frequency details. This inherent bias (Rahaman et al. 2019; Xu 2020) degrades visual quality and negatively impacts overall fusion performance. Moreover, the inefficiency of regularization strategies (Xiao et al. 2024; Fuoli, Van Gool, and Timofte 2021) may lead to the loss of critical high-frequency information, hindering the recovery of textures and edges in the results. To address these limitations, we propose SMC-Mamba, a Self-supervised Multiplex Consensus Mamba for general image fusion. This framework comprises three core designs: a Modality-Agnostic Feature Enhancement module (MAFE), a Multiplex Consensus Cross-modal Mamba module (MCCM), and the Bi-level Self-supervised Contrastive Learning Loss (BSCL).

Initially, to achieve high-quality fusion results with abundant intricate details and boost performance in downstream tasks, we design the task-agnostic BSCL regularization loss, which reinforces high-frequency textures and structures without increasing complexity. Specifically, the high-frequency components of the fused images are drawn towards to those of the input modalities, while being pushed away from their low-frequency components at both the fea-

ture and pixel levels within the latent spaces.

To effectively handle diverse fusion tasks, we propose the MCCM module, which encourages diverse feature preferences and fusion strategies across experts, while enabling dynamically activated experts to collaborate and converge toward a unified representation, thereby providing reliable results for image fusion and downstream tasks. Additionally, unlike convolutions or self-attention, Mamba employs a scanning scheme to capture long-range dependencies in a content-aware manner. However, poorly designed scans may separate adjacent pixels in sequence, disrupting feature continuity. Existing methods focus mainly on spatial scanning (Zhu et al. 2024a) or single-modal scenarios (Peng et al. 2024; Xie et al. 2024), neglecting spatial-channel interactions and cross-modal dependencies. To address this, we introduce a cross-modal scanning mechanism within each MCCM expert, enhancing inter-modal feature exchange and enabling seamless fusion of complementary cues.

Furthermore, although SSMs effectively capture long-range context, they often struggle with preserving local details. To address this, we introduce the MAFE module, which integrates local and global branches. The local branch uses a gating mechanism to adaptively extract fine-grained spatial features, while the global branch leverages Mamba with spatial-channel and frequency-rotational scanning to enhance global representations. This design captures long-range spatial-channel correlations and frequency relationships, enabling efficient modeling of global context while retaining local precision and enhancing unimodal feature representations.

In summary, the contributions of our work are as follows:

- We propose SMC-Mamba, a Self-supervised Multiplex Consensus Mamba for general image fusion. This approach aims to dynamically and efficiently integrate complementary information from various modalities, flexibly handling different image fusion tasks.

- We devise the MCCM module, which promotes diverse feature preferences and fusion strategies across experts and enables activated experts to converge toward a unified representation, thereby providing reliable results for image fusion and downstream tasks.

- We design a novel self-supervised BSCL regularization loss that enhances the preservation of high-frequency information at both feature and pixel levels without increasing model complexity, while also improving performance in downstream visual tasks.

- We introduce the cross-modal scanning to exploit long-range cross-modal dependencies, strengthening feature interactions and facilitating the seamless integration of complementary and critical information from both modalities.

Methodology

In this section, we provide an in-depth overview of our proposed SMC-Mamba framework, as illustrated in Figure 1. The SMC-Mamba framework comprises three core components: MAFE, MCCM, and the BSCL approach. The details are illustrated as below.

Modality-Agnostic Feature Enhancement

Given source images $I_{mk} \in \mathbb{R}^{H \times W \times C_k}$ from tasks like IVIF, MDIF, MFIF, and MEIF (with modality index $k \in \{1, 2\}$), we extract shallow features F_{sk} using a 3×3 convolution and layer normalization:

$$F_{sk} = \text{LN}\left(\text{Conv}_{3 \times 3}\left(I_{mk}\right)\right). \tag{1}$$

Local Branch. The shallow features $F_{sk} \in \mathbb{R}^{H \times W \times C}$ are first divided into patches $F_{sk}^j \in \mathbb{R}^{\frac{H}{2} \times \frac{W}{2} \times C}$ via tokenization. Each patch is processed with a 3×3 depth-wise convolution and then passed through a gating unit to adaptively capture local fine-grained details:

$$F_{sk}^j = \text{Token}\left(F_{sk}\right), \tag{2}$$

$$F_{sk}^{j-dw} = \text{DWConv}_{3 \times 3}\left(F_{sk}^j\right), \tag{3}$$

where $\text{Token}(\cdot)$ refers to the tokenization process, dividing the input shallow features F_{sk} into smaller patches, and j denotes the patch index.

Next, a GELU non-linearity (Hendrycks and Gimpel 2016) is applied to generate an attention map, which adaptively modulates F_{sk}^{j-dw} via element-wise multiplication:

$$F_L = \text{Gate}\left(\text{Conv}_{1 \times 1}\left(F_{sk}^{j-dw}\right)\right) \odot F_{sk}^{j-dw}, \tag{4}$$

where $\text{Conv}_{1 \times 1}(\cdot)$ denotes 1×1 convolution, $\text{Gate}(\cdot)$ represents the gate function, and $\odot$ is the element-wise product.

Global Branch. In the spatial-channel SSM, input features F_{sk} are fed into two parallel sub-branches: one applies a SiLU activation directly, while the other performs a 1×1 convolution followed by a 3×3 depth-wise convolution, both activated by SiLU. The outputs are then scanned using the spatial-channel scanning SC-Scan$(\cdot)$:

$$F_{DW} = \text{DWConv}_{3 \times 3}\left(\text{Conv}_{1 \times 1}\left(F_{sk}\right)\right), \tag{5}$$

$$F_{spa}^{sub1} = \text{LN}\left(\text{SC-Scan}\left(\text{SiLU}\left(F_{DW}\right)\right)\right), \tag{6}$$

$$F_{spa} = F_{spa}^{sub1} \odot \text{SiLU}\left(F_{sk}\right). \tag{7}$$

In Fourier theory, modifying a single point in the frequency domain has a global impact on all input features. To enhance global representation, the frequency-rotational SSM processes F_{sk} via two sub-branches: one applies SiLU activation directly, while the other transforms F_{sk} into the frequency domain using the discrete Fourier transform (DFT):

$$\mathcal{F}(F_{sk})(u, v) = \sum_{h=0}^{H-1} \sum_{w=0}^{W-1} F_{sk}(h, w) \cdot e^{-j2\pi\left(\frac{uh}{H} + \frac{vw}{W}\right)}, \tag{8}$$

where u and v denote the coordinates in the Fourier space, $\mathcal{F}(\cdot)$ represents the Fourier transformation.

The amplitude and phase components, $\mathcal{A}\left(F_{sk}\right)$ and $\mathcal{P}\left(F_{sk}\right)$, can be derived from the Fourier transform:

$$\mathcal{A}\left(F_{sk}\right), \mathcal{P}\left(F_{sk}\right) = \mathcal{F}\left(F_{sk}\right). \tag{9}$$

Then, a 3×3 depth-wise convolution and SiLU activation are applied to the amplitude and phase, followed by the frequency-rotational scanning FR-Scan$(\cdot)$:

$$F_{fre}^{\mathcal{A}} = \text{FR-Scan}\left(\text{SiLU}\left(\text{DWConv}_{3 \times 3}\left(\mathcal{A}\left(F_{sk}\right)\right)\right)\right), \tag{10}$$
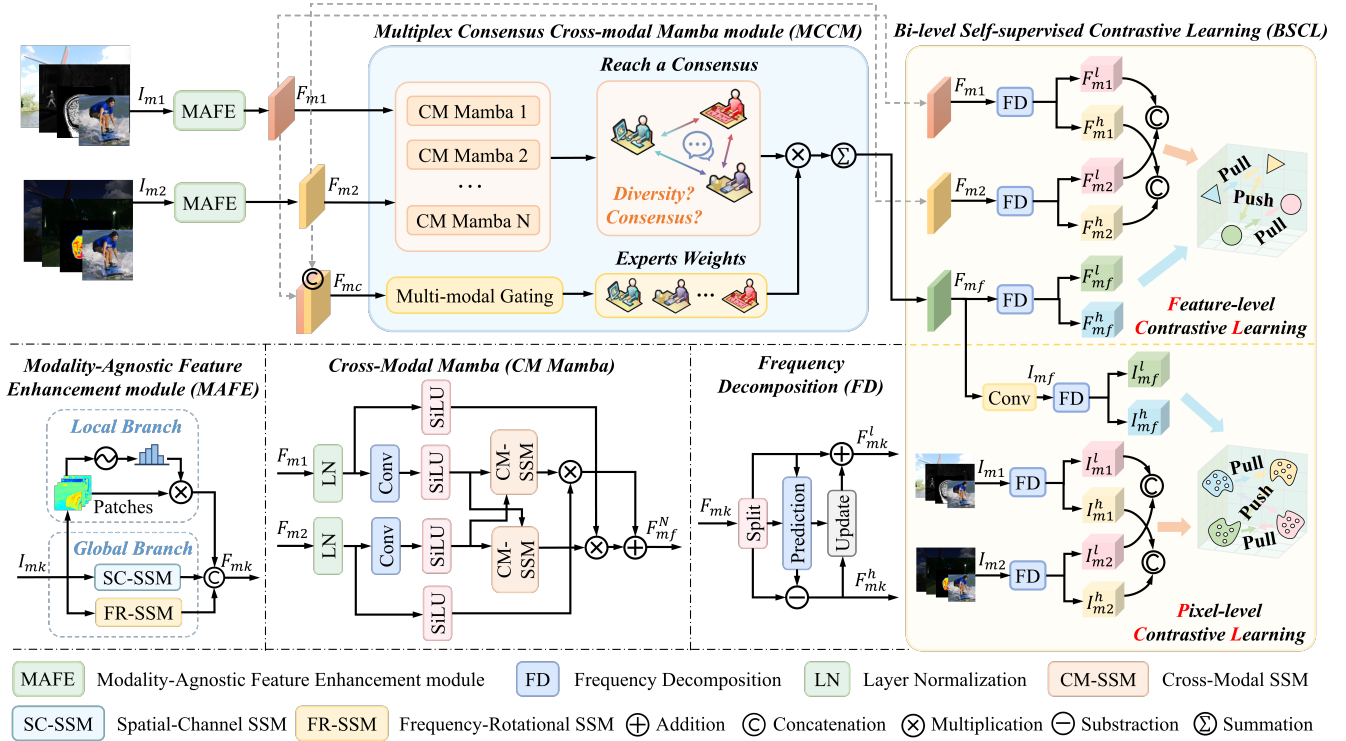
Figure 1: The overall framework of our proposed network, which consists of three main components: 1) Modality-Agnostic Feature Enhancement module (MAFE). 2) Multiplex Consensus Cross-modal Mamba module (MCCM). 3) Bi-level Self-supervised Contrastive Learning Loss (BSCL).

$$F_{fre}^{\mathcal{P}} = \text{FR-Scan}\left(\text{SiLU}\left(\text{DWConv}_{3\times3}\left(\mathcal{P}\left(F_{sk}\right)\right)\right)\right). \quad (11)$$

Next, the amplitude and phase features are transformed back to the spatial domain via inverse discrete Fourier transform (IDFT):

$$F_{fre} = \mathcal{F}^{-1}\left(F_{fre}^{\mathcal{A}}, F_{fre}^{\mathcal{P}}\right) \odot \text{SiLU}(F_{sk}), \quad (12)$$

where $\mathcal{F}^{-1}(\cdot)$ denotes the IDFT operation.

After that, the global features can be derived as below:

$$F_G = \text{Cat}\left(F_{spa}, F_{fre}\right), \quad (13)$$

where $\text{Cat}(\cdot)$ is the concatenating function.

By integrating complementary local and global features, the MAFE module enhances modality-agnostic representation, enabling efficient long-range context capture while preserving local detail. The output features are as follows:

$$F_{mk} = \text{Cat}\left(F_L, F_G\right), \quad (14)$$

where k represents the index of each modality, with values of 1 and 2.

Cross-modal Scanning. To enhance cross-modal feature interaction and aggregate complementary information, we propose cross-modal scanning $\text{CM-Scan}(\cdot)$, comprising spatial and channel interaction scanning across modalities. Spatial scanning performs forward and reverse passes between modalities to model long-range spatial correlations, while channel scanning alternates across modalities to capture inter-modal dependencies. This strategy produce a more comprehensive and informative fused results.

Algorithm 1: Cross-modal Mamba Architecture

Input: Enhanced modality-agnostic features F_{m1} and F_{m2}
Output: Cross-modal Mamba fusion result F_{mf}^N

1: /* Layer normalization and reshape */
2: $F_{ln1} \leftarrow \text{Linear}\left(\text{LN}(F_{m1})\right)$
3: $F_{ln2} \leftarrow \text{Linear}\left(\text{LN}(F_{m2})\right)$
4: /* 1×1 convolution followed by SiLU activation */
5: $F_{silu1} \leftarrow \text{SiLU}\left(\text{Conv}_{1\times1}(F_{ln1})\right)$
6: $F_{silu2} \leftarrow \text{SiLU}\left(\text{Conv}_{1\times1}(F_{ln2})\right)$
7: /* Cross-modal scanning CM-Scan$(\cdot)$ */
8: $F_{cm1} \leftarrow \text{CM-Scan}(F_{silu1}, F_{silu2})$
9: $F_{cm2} \leftarrow \text{CM-Scan}(F_{silu2}, F_{silu1})$
10: /* Cross-modal feature interactions and fusion */
11: $F_{mf}^N \leftarrow F_{cm1} \odot \text{SiLU}(F_{ln2}) + F_{cm2} \odot \text{SiLU}(F_{ln1})$

Return F_{mf}^N

Multiplex Consensus Cross-modal Mamba module

To effectively capture complex cross-modal correlations, we propose the Multiplex Consensus Cross-modal Mamba (MCCM) module, which integrates multiple cross-modal Mamba experts $\{\text{CM}_1, \ldots, \text{CM}_N\}$ under a unified gating framework. Each expert performs independent cross-modal fusion, while the gating network adaptively determines their importance based on input content.

Given modality-agnostic features F_{mk} ($k \in \{1, 2\}$), we concatenate them into F_{mc} and pass it through the gating network. Global Average Pooling (GAP) and Global Max

Algorithm 2: Frequency Decomposition
___

Input: Enhanced modality-agnostic features F_{mk}, fused feature F_{mf}, input images I_{mk}, and fused image I_{mf}

Output: Feature-level low-frequency components F_{mk}^l and F_{mf}^l, high-frequency residuals F_{mk}^h and F_{mf}^h, image-level low-frequency components I_{mk}^l and I_{mf}^l, high-frequency residuals I_{mk}^h and I_{mf}^h

1: /* Feature-level. Channel-wise Split S(·). */
2: $F_{c1}, F_{c2} \leftarrow \text{S}(F_{mk})$
3: $F_{cf1}, F_{cf2} \leftarrow \text{S}(F_{mf})$
4: /* Prediction P(·) for high-frequency residual */
5: $F_{mk}^h \leftarrow F_{c2} - \text{P}(F_{c1})$
6: $F_{mf}^h \leftarrow F_{cf2} - \text{P}(F_{cf1})$
7: /* Update U(·) for low-frequency refinement */
8: $F_{mk}^l \leftarrow F_{c1} + \text{U}(F_{mk}^h)$
9: $F_{mf}^l \leftarrow F_{cf1} + \text{U}(F_{mf}^h)$
10: /* Image-level. Channel-wise Split S(·). */
11: $I_{c1}, I_{c2} \leftarrow \text{S}(I_{mk})$
12: $I_{cf1}, I_{cf2} \leftarrow \text{S}(I_{mf})$
13: /* Prediction P(·) for high-frequency residual */
14: $I_{mk}^h \leftarrow I_{c2} - \text{P}(I_{c1})$
15: $I_{mf}^h \leftarrow I_{cf2} - \text{P}(I_{cf1})$
16: /* Update U(·) for low-frequency refinement */
17: $I_{mk}^l \leftarrow I_{c1} + \text{U}(I_{mk}^h)$
18: $I_{mf}^l \leftarrow I_{cf1} + \text{U}(I_{mf}^h)$

Return $F_{mk}^h, F_{mk}^l, F_{mf}^h, F_{mf}^l, I_{mk}^h, I_{mk}^l, I_{mf}^h, I_{mf}^l$
___

Pooling (GMP) are first applied to extract representative global features:

$$F_{mc} = \text{Cat}(F_{m1}, F_{m2}), \qquad (15)$$

$$F_g = \text{GAP}(F_{mc}) + \text{GMP}(F_{mc}). \qquad (16)$$

A learnable noise term ϵ is added, controlled by $\text{Softplus}(\cdot)$ to ensure non-negative noise for stable activation:

$$\epsilon = \mathcal{N}(0,1) \cdot \text{Softplus}(F_g \cdot W_{\text{noise}}). \qquad (17)$$

The expert weights are computed as:

$$W_{\text{exp}} = \text{Softmax}\left(\text{TopK}(F_g \cdot W_g + \epsilon)\right), \qquad (18)$$

only the top-k experts ($k = 2$) are activated, the unselected experts receive zero weight. The added learnable noise introduces randomness, encouraging balanced expert selection.

During training, all experts are used with weights from W_{exp} to guide learning. At inference, only the top-k experts are executed, enabling efficient, task-adaptive computation.

Each expert follows a cross-modal Mamba architecture (Figure 1) that includes layer normalization, linear projection, a 1×1 convolution with SiLU activation, and the proposed cross-modal scanning operator $\text{CM-Scan}(\cdot)$ to enable rich inter-modal interactions. The full process is detailed in Algorithm 1. The output of MCCM is the weighted sum of expert outputs:

$$F_{mf} = \sum_{i=1}^{N} W_{\text{exp}}^i \cdot \text{CM}_i(F_{mc}), \qquad (19)$$

where $\text{CM}_i(\cdot)$ represents the i-th cross-modal Mamba expert network. N denotes the number of experts, with N set to 4.

Workload Balancing Loss. To prevent gating collapse and ensure all experts contribute during training, we introduce a load balancing loss based on the coefficient of variation:

$$\mathcal{L}_{\text{wb}} = \left(\frac{\sigma(W_{\text{exp}})}{\overline{W_{\text{exp}}}}\right)^2, \qquad (20)$$

where $\sigma(\cdot)$ and $\overline{(\cdot)}$ denote the standard deviation and mean of expert weights, respectively.

Expert Diversity Loss. To encourage heterogeneous expert behavior, we propose the expert diversity loss $\mathcal{L}_{\text{div}}$, which promotes diverse feature preferences and fusion strategies across expert, fostering a complementary and specialized ensemble:

$$\mathcal{L}_{\text{div}} = \frac{1}{N(N-1)} \sum_{i \neq j} \cos\left(\hat{F}_i, \hat{F}_j\right), \qquad (21)$$

where $\hat{F}_i = \text{CM}_i(F_{mc})$ is the output of the i-th cross-modal Mamba expert, $\cos(\hat{F}_i, \hat{F}_j)$ denotes the cosine similarity between expert outputs, N is the total number of experts. Lower similarity indicates stronger diversity.

Consensus Loss. To ensure consistent fusion outputs, we also encourage the activated experts to converge toward a unified representation, thereby providing reliable results for image fusion and downstream tasks. The consensus feature is computed as the weighted average of expert outputs:

$$F_{\text{consensus}} = \sum_{i=1}^{N} W_{\text{exp}}^i \cdot \hat{F}_i. \qquad (22)$$

The consensus loss $\mathcal{L}_{\text{cons}}$ penalizes deviations from this aggregated representation:

$$\mathcal{L}_{\text{cons}} = \sum_{i=1}^{N} W_{\text{exp}}^i \cdot \left\|\hat{F}_i - F_{\text{consensus}}\right\|_2^2. \qquad (23)$$

Joint Objective. To balance expert specialization and collaboration, we combine these objectives with a time-decayed weighting scheme:

$$\mathcal{L}_{\text{mccm}} = \mathcal{L}_{\text{wb}} + \lambda(t) \cdot \mathcal{L}_{\text{div}} + (1 - \lambda(t)) \cdot \mathcal{L}_{\text{cons}}, \qquad (24)$$

where $\lambda(t) = \cos\left(\frac{t}{T} \cdot \frac{\pi}{2}\right)$ decays over epochs (t is the current epoch, T denotes the total epochs), prioritizing diversity in the early stages and consensus in later stages. This dynamic balance enables the expert ensemble to first explore diverse fusion strategies and then consolidate into robust and aligned representations.

Bi-level Self-supervised Contrastive Learning Loss

For general image fusion, enhancing high-frequency detail without increasing model complexity remains challenging. To tackle this, we propose a Bi-level Self-supervised Contrastive Learning Loss (BSCL) that constrains high-frequency representations at both feature and pixel levels.

Specifically, we use the Haar wavelet lifting scheme (Sweldens 1998) to decompose fused and modality-enhanced features into high- and low-frequency
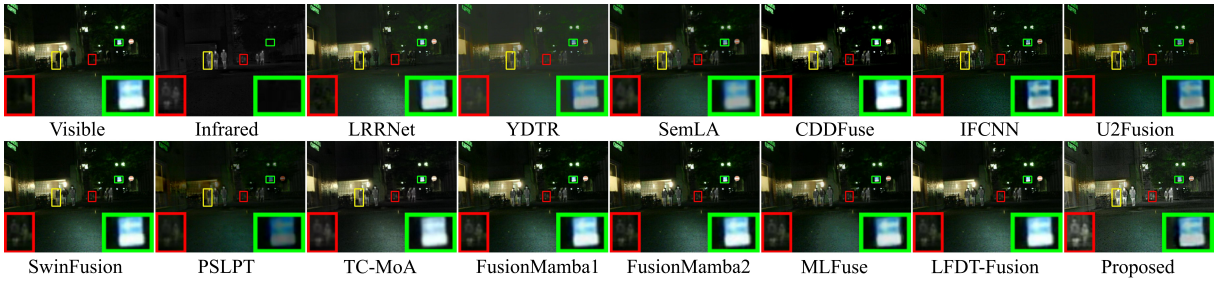
Figure 2: Visual comparisons of all the compared approaches on the MSRS dataset in IVIF task.
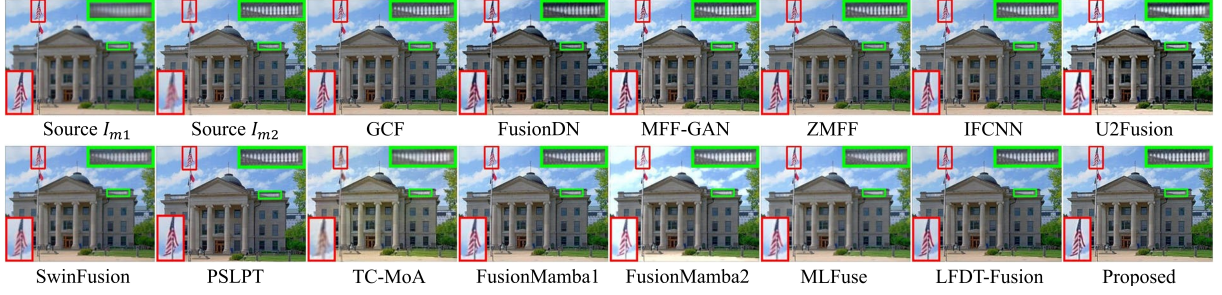

Figure 3: Visual comparisons of all the compared approaches on the MFI-WHU dataset in MFIF task.

components, as shown in Figure 1. The enhanced modality-agnostic feature F_{mk} is split into two subsets, F_{c1} and F_{c2}, via a channel-wise split operation $\mathrm{S}(\cdot)$.

Since F_{c1} and F_{c2} originate from the same source, they are strongly correlated. The Prediction block $\mathrm{P}(\cdot)$ uses the coarse low-frequency component F_{c1} to predict the fine-grained high-frequency F_{c2}, yielding the high-frequency residual F_{mk}^{h}. The Update block $\mathrm{U}(\cdot)$ then refines F_{c1} using feedback from F_{mk}^{h}, producing the updated low-frequency component F_{mk}^{l}.

A similar decomposition is applied to the fused feature F_{mf}, generating F_{mf}^{h} and F_{mf}^{l}. At the image level, the fused image I_{mf} and source images I_{mk} are also decomposed using the Haar wavelet lifting scheme. The complete process is outlined in Algorithm 2.

Feature-level Contrastive Learning. Given the fused feature F_{mf} and the enhanced modality-agnostic features F_{mk}, BSCL aims to pull the fused high-frequency components F_{mf}^{h} closer to F_{mk}^{h} while pushing them away from the low-frequency components F_{mk}^{l} in latent space. We begin by concatenating the high- and low-frequency components of the input modalities:

$$F_{mc}^{h} = \mathrm{Cat}\left(F_{m1}^{h}, F_{m2}^{h}\right), \qquad (25)$$

$$F_{mc}^{l} = \mathrm{Cat}\left(F_{m1}^{l}, F_{m2}^{l}\right). \qquad (26)$$

Then, the feature-level contrastive constraint is defined as:

$$\mathcal{L}_{\mathrm{fcl}} = \frac{\left\| F_{mf}^{h} - F_{mc}^{h} \right\|_{1}^{2}}{\left\| F_{mf}^{h} - F_{mc}^{l} \right\|_{1}^{2}} + \frac{\left\| F_{mf}^{l} - F_{mc}^{l} \right\|_{1}^{2}}{\left\| F_{mf}^{l} - F_{mc}^{h} \right\|_{1}^{2}}. \qquad (27)$$

Pixel-level Contrastive Learning. Similarly, given the fused image I_{mf} and input images I_{mk}, pixel-level con-

trastive learning pulls the fused high-frequency components I_{mf}^{h} closer to I_{mk}^{h} and pushes them away from I_{mk}^{l}. We first concatenate the high and low-frequency components of the input images:

$$I_{mc}^{h} = \mathrm{Cat}\left(I_{m1}^{h}, I_{m2}^{h}\right), \qquad (28)$$

$$I_{mc}^{l} = \mathrm{Cat}\left(I_{m1}^{l}, I_{m2}^{l}\right). \qquad (29)$$

The pixel-level contrastive constraint is defined as:

$$\mathcal{L}_{\mathrm{pcl}} = \frac{\left\| I_{mf}^{h} - I_{mc}^{h} \right\|_{1}^{2}}{\left\| I_{mf}^{h} - I_{mc}^{l} \right\|_{1}^{2}} + \frac{\left\| I_{mf}^{l} - I_{mc}^{l} \right\|_{1}^{2}}{\left\| I_{mf}^{l} - I_{mc}^{h} \right\|_{1}^{2}}. \qquad (30)$$

Overall Loss Function

The overall loss function is defined as follows:

$$\mathcal{L}_{\mathrm{total}} = \lambda_1 \mathcal{L}_{\mathrm{fcl}} + \lambda_2 \mathcal{L}_{\mathrm{pcl}} + \lambda_3 \mathcal{L}_{\mathrm{mccm}} + \lambda_4 \mathcal{L}_{\mathrm{ssim}} + \lambda_5 \mathcal{L}_{\mathrm{int}}, \qquad (31)$$

where the hyperparameters λ_1 to λ_5 control the contribution of each sub-loss term and are empirically set to 0.8, 0.4, 1, 1, and 1, respectively. $\mathcal{L}_{\mathrm{ssim}}$ denotes the SSIM loss (Wang et al. 2004), and $\mathcal{L}_{\mathrm{int}}$ represents the intensity loss as introduced in (Zhang et al. 2020).

Experiment

Implementation Details

We implement our model using PyTorch and train it on a single NVIDIA RTX 3090 GPU. The ADAM optimizer with $\beta = 0.9$ is used with a batch size of 1 and an initial learning rate of 2×10^{-4}, which is halved every 1000 iterations via cosine annealing. In MCCM, we use $N = 4$ cross-modal Mamba experts.

Datasets

For the IVIF task, we train on the MSRS (Tang et al. 2022) dataset and test on MSRS, RoadScene (Xu et al. 2020c), and M³FD (Liu et al. 2022a). MSRS and M³FD are also used for downstream detection evaluation, while MSRS is used for segmentation. For medical image fusion, we utilize the Harvard medical dataset, which includes CT-MRI, PET-MRI, and SPECT-MRI tasks, each used independently for both training and testing. For multi-focus fusion, the MFI-WHU (Zhang et al. 2021) dataset is used for training, with testing on both Lytro (Nejati, Samavi, and Shirani 2015) and MFI-WHU. For multi-exposure fusion, we train on the MEF (Cai, Gu, and Zhang 2018) dataset and test on the MEF benchmark (Zhang 2021).

Comparison Methods and Evaluation Metrics

We conduct comparisons with several SOTA techniques, including both general image fusion frameworks and task-specific approaches. Specifically, nine unified image fusion frameworks include IFCNN (Zhang et al. 2020), U2Fusion (Xu et al. 2020b), SwinFusion (Ma et al. 2022), PSLPT (Wang, Deng, and Vivone 2024), TC-MoA (Zhu et al. 2024b), Fusionmamba1 (Peng et al. 2024), Fusionmamba2 (Xie et al. 2024), MLFuse (Lei et al. 2025), and LFDT-Fusion (Yang et al. 2025). In addition, we also compare with task-specific methods. LRRNet (Li et al. 2023), YDTR (Tang, He, and Liu 2023), SemLA (Xie et al. 2023), and CDDFuse (Zhao et al. 2023b) for IVIF task. EMFusion (Xu and Ma 2021), MSRPAN (Fu et al. 2021), TU-Fusion (Zhao et al. 2023a) and ALMFnet (Mu et al. 2024) for MDIF. GCF (Xu et al. 2020a), FusionDN (Xu et al. 2020c), MFF-GAN (Zhang et al. 2021) and ZMFF (Hu et al. 2023) for MFIF. DPE-MEF (Han et al. 2022), AGAL (Liu et al. 2022b), BHF-MEF (Mu et al. 2023) and SAMT-MEF (Huang et al. 2024) for MEIF task.

For evaluation metrics, we select several non-reference metrics to measure the fusion results, including mutual information (MI), spatial frequency (SF), average gradient (AG), correlation coefficient (CC), sum of the correlations of differences (SCD), visual information fidelity (VIF), edge based similarity measurement (Q_{abf}), multi-scale structural similarity index measure (MS-SSIM), and noise or artifacts added in fused image due to fusion process (N_{abf}).

Quantitative Comparison with SOTA Methods

Tables 1 and 2 present the quantitative results for the IVIF and MFIF tasks. The IVIF task is evaluated on the MSRS, RoadScene, and M³FD datasets, and the MFIF task is assessed on the Lytro and MFI-WHU datasets. Our proposed method consistently outperforms existing approaches across nearly all metrics and datasets.

Visual Quality Comparison with SOTA Methods

The visual comparisons for the IVIF task are provided in Figure 2. Only our method clearly highlights pedestrian targets within the red box. Figure 3 illustrates the MFIF fusion results. Our method preserves fine-grained textures, such as sharp railings and clear flag lines, while maintaining accurate color fidelity, demonstrating superior visual quality.

	Methods	MI↑	SF↑	AG↑	CC↑	SCD↑	VIF↑	Q_{abf}↑	MS_SSIM↑
MSRS / Task-spec	LRRNet	2.922	8.472	2.651	0.515	0.791	0.541	0.454	0.373
	YDTR	2.760	7.404	2.201	0.631	1.138	0.577	0.349	0.441
	SemLA	2.442	6.339	2.239	0.641	1.392	0.608	0.290	0.498
	CDDFuse	3.657	12.083	4.043	0.596	1.549	0.819	0.548	0.459
MSRS / General	IFCNN	1.796	12.134	4.030	0.633	1.374	0.579	0.479	0.504
	U2Fusion	2.183	9.242	2.899	0.632	1.258	0.512	0.391	0.440
	SwinFusion	3.652	11.038	3.546	0.595	1.647	0.825	0.558	0.504
	PSLPT	2.284	10.419	3.306	0.610	1.374	0.753	0.553	0.501
	TC-MoA	3.251	9.370	3.251	0.613	1.661	0.811	0.565	0.515
	Fusionmamba1	4.121	10.955	3.599	0.611	1.635	0.974	0.652	0.511
	Fusionmamba2	3.608	11.401	3.658	0.610	1.645	0.947	0.637	0.520
	MLFuse	2.889	8.819	2.962	0.634	1.520	0.753	0.519	0.498
	LFDT-Fusion	4.216	11.236	3.694	0.600	1.637	0.876	0.624	0.512
	Proposed	**4.490**	**12.211**	**4.054**	**0.699**	**1.664**	**0.991**	**0.658**	**0.522**
RoadScene / Task-spec	LRRNet	2.704	11.114	4.166	0.621	1.430	0.488	0.323	0.537
	YDTR	3.043	10.788	4.035	0.591	1.229	0.602	0.463	0.524
	SemLA	2.808	15.571	4.899	0.606	1.269	0.564	0.415	0.518
	CDDFuse	3.001	**19.779**	**7.029**	0.623	1.707	0.610	0.450	0.515
RoadScene / General	IFCNN	2.842	15.994	6.304	0.637	1.558	0.591	0.536	0.542
	U2Fusion	2.578	15.282	6.099	0.630	1.605	0.564	0.506	0.546
	SwinFusion	3.334	12.161	4.516	0.623	1.576	0.614	0.450	0.534
	PSLPT	2.001	9.172	3.639	0.625	1.009	0.134	0.171	0.238
	TC-MoA	2.853	12.786	5.339	0.611	1.562	0.577	0.477	0.522
	Fusionmamba1	3.189	14.659	5.602	0.632	1.322	0.635	0.543	0.519
	Fusionmamba2	3.213	15.844	5.711	0.624	1.580	0.621	0.496	0.538
	MLFuse	2.948	13.272	5.094	0.640	1.595	0.629	0.527	0.545
	LFDT-Fusion	3.642	13.997	5.215	0.623	1.209	0.624	0.529	0.523
	Proposed	3.772	17.971	6.866	**0.643**	**1.733**	**0.642**	**0.557**	**0.547**
M³FD / Task-spec	LRRNet	2.892	11.162	3.700	0.522	1.726	0.556	0.510	0.418
	YDTR	3.034	7.586	2.748	0.521	1.509	0.470	0.302	0.477
	SemLA	2.376	7.285	3.181	0.480	1.495	0.542	0.363	0.473
	CDDFuse	3.994	17.578	5.706	0.511	1.673	0.802	0.613	0.460
M³FD / General	IFCNN	2.630	16.250	5.448	0.554	1.710	0.685	0.590	0.445
	U2Fusion	2.683	14.248	5.179	0.539	1.753	0.673	0.578	0.463
	SwinFusion	4.020	14.415	4.798	0.500	1.588	0.746	0.616	0.492
	PSLPT	4.563	6.439	2.107	0.638	0.638	0.958	0.321	0.483
	TC-MoA	2.856	11.221	4.010	0.506	1.556	0.579	0.508	0.466
	Fusionmamba1	4.044	14.042	4.689	0.465	1.414	0.747	0.580	0.480
	Fusionmamba2	3.823	14.933	4.913	0.492	1.540	0.744	0.600	0.496
	MLFuse	2.897	10.229	3.382	0.560	1.600	0.592	0.460	0.501
	LFDT-Fusion	3.920	15.040	4.958	0.446	1.352	0.874	0.624	0.486
	Proposed	4.280	**19.495**	**6.378**	**0.561**	**1.791**	**0.972**	**0.632**	**0.507**

Table 1: Average metrics of all methods on the IVIF task. **Bold** and underlined values indicate the best and second-best scores, respectively.

	Methods	MI↑	SF↑	AG↑	CC↑	SCD↑	VIF↑	N_{abf}↓	MS_SSIM↑
Lytro / Task-spec	GCF	**7.438**	19.399	6.811	0.971	0.539	1.259	0.010	0.891
	FusionDN	5.793	17.129	6.359	0.917	0.511	1.007	0.030	0.866
	MFF-GAN	6.066	21.037	7.394	0.972	0.755	1.099	0.051	0.877
	ZMFF	6.630	18.770	6.715	0.971	0.442	1.175	0.028	0.890
Lytro / General	IFCNN	6.896	19.398	7.254	0.967	0.606	1.258	0.026	0.835
	U2Fusion	5.787	19.634	6.840	0.973	0.546	1.255	0.060	0.890
	SwinFusion	6.149	16.941	6.116	0.873	**0.837**	1.069	0.027	0.862
	PSLPT	3.201	18.766	6.686	0.810	0.308	0.207	0.105	0.445
	TC-MoA	5.356	14.593	5.502	0.962	0.506	1.040	0.030	0.849
	Fusionmamba1	6.426	17.973	6.523	0.975	0.762	1.163	0.022	0.882
	Fusionmamba2	5.836	17.104	6.179	0.971	0.760	1.046	0.024	0.842
	MLFuse	5.965	14.032	5.179	0.981	0.684	1.028	0.008	0.892
	LFDT-Fusion	6.906	19.074	6.631	0.973	0.546	1.264	0.016	0.896
	Proposed	7.081	**23.785**	**8.191**	**0.989**	0.787	**1.339**	**0.007**	**0.899**
MFI-WHU / Task-spec	GCF	**7.269**	26.577	8.146	0.966	0.537	1.326	0.073	0.942
	FusionDN	5.351	24.029	8.469	0.961	0.884	1.012	0.083	0.846
	MFF-GAN	5.684	29.438	9.447	0.961	0.964	1.120	0.089	0.900
	ZMFF	5.780	24.347	8.105	0.950	0.405	1.053	0.074	0.923
MFI-WHU / General	IFCNN	6.670	26.474	8.254	0.967	0.606	1.258	0.084	0.935
	U2Fusion	5.151	24.177	8.727	0.965	**1.094**	1.018	0.093	0.861
	SwinFusion	6.160	16.682	5.755	0.979	0.418	1.123	0.111	0.932
	PSLPT	3.257	25.277	8.049	0.777	0.285	0.287	0.109	0.511
	TC-MoA	4.820	16.037	6.134	0.960	0.544	0.978	0.072	0.891
	Fusionmamba1	5.854	22.311	7.653	0.974	0.957	1.125	0.076	0.922
	Fusionmamba2	5.371	23.218	7.536	0.966	0.964	1.024	0.081	0.848
	MLFuse	5.581	20.500	6.686	0.977	0.801	1.044	0.080	0.924
	LFDT-Fusion	6.649	25.316	8.041	0.971	0.597	1.270	0.073	0.943
	Proposed	6.890	**35.669**	**10.929**	**0.985**	0.972	**1.344**	0.070	**0.948**

Table 2: Average metrics of all methods on the MFIF task.

Ablation	Configuration	Params (M)	FLOPs (G)	Inference Time (ms)	MSRS Dataset							
					MI↑	SF↑	AG↑	CC↑	SCD↑	VIF↑	Q_{abf}↑	MS-SSIM↑
Proposed	-	0.149	46.105	288.545	**4.490**	12.211	4.054	**0.699**	**1.664**	**0.991**	**0.658**	**0.522**
Core Operations	Mamba → Conv	0.325	78.843	430.392	3.190	12.126	4.022	0.626	1.610	0.735	0.529	0.509
	Mamba → Window Attention	0.392	58.313	792.461	3.780	11.463	3.113	0.406	1.415	0.672	0.454	0.459
	Mamba → Self Attention	0.240	60.747	1271.691	3.710	**12.387**	**4.180**	0.601	1.630	0.834	0.588	0.518
Main Modules	MAFE Module → None	0.041	14.260	226.355	2.384	12.073	4.023	0.638	1.544	0.803	0.548	0.515
	MCCM Module → None	0.125	38.606	164.867	2.202	10.048	3.426	0.544	1.392	0.702	0.496	0.453
Loss Functions	w/o $\mathcal{L}_{fcl}$	-	-	-	3.914	11.147	3.717	0.585	1.546	0.946	0.624	0.517
	w/o $\mathcal{L}_{pcl}$	-	-	-	3.870	10.952	3.627	0.572	1.522	0.937	0.613	0.511
	w/o $\mathcal{L}_{fcl}$ & $\mathcal{L}_{pcl}$	-	-	-	3.721	10.823	3.580	0.565	1.482	0.925	0.601	0.503
	w/o $\mathcal{L}_{wb}$	-	-	-	3.840	11.142	3.804	0.596	1.583	0.947	0.632	0.510
	w/o $\mathcal{L}_{div}$	-	-	-	3.601	10.997	3.697	0.582	1.560	0.929	0.614	0.500
	w/o $\mathcal{L}_{cons}$	-	-	-	3.702	11.060	3.727	0.590	1.571	0.938	0.626	0.506
	w/o $\mathcal{L}_{mccm}$	-	-	-	3.466	10.891	3.643	0.563	1.504	0.906	0.598	0.496
Scanning Schemes	w/o Spatial-channel scanning	-	-	-	4.106	11.381	3.587	0.618	1.554	0.936	0.641	0.516
	w/o Frequency-rotational scanning	-	-	-	4.350	11.942	4.021	0.620	1.515	0.963	0.642	0.513
	w/o Cross-modal scanning	-	-	-	3.965	11.191	3.538	0.557	1.470	0.896	0.601	0.504
Scanning Directions	Bi-direction → Single direction	-	-	-	4.270	12.080	4.013	0.670	1.639	0.932	0.621	0.513

Table 3: Ablation study for SMC-Mamba on the MSRS dataset. "A → B" means replacing A with B. The thop library counts the number of parameters and FLOPs at a resolution of 480×640 pixels. Best results are highlighted in **bold**.

	Methods	Background	Car	Person	Bike	Curve	Barrier	mIoU
Source	IR	97.9	85.0	51.0	69.7	51.3	68.9	70.6
	VIS	97.9	86.7	39.5	70.4	53.2	71.4	69.9
Task-spec	LRRNet	98.3	88.9	67.7	69.1	51.9	71.5	74.6
	YDTR	98.5	89.6	72.0	70.9	62.0	73.3	77.7
	SemLA	98.4	89.6	70.8	70.0	58.2	75.0	77.0
	CDDFuse	98.5	89.7	74.2	71.4	63.8	73.7	78.6
General	IFCNN	98.4	88.8	71.3	71.7	57.7	71.3	76.5
	U2Fusion	98.4	88.3	71.3	71.2	58.8	71.1	76.5
	SwinFusion	98.6	89.9	73.6	72.3	64.7	73.3	78.7
	PSLPT	98.5	89.8	73.7	71.8	59.4	75.7	78.2
	TC-MoA	98.5	89.8	72.6	70.8	63.8	74.3	78.3
	Fusionmamba1	98.4	88.8	71.3	67.8	61.8	71.1	76.5
	Fusionmamba2	98.5	89.9	72.9	70.0	63.3	74.6	78.2
	MLFuse	98.5	89.9	73.6	71.0	63.8	75.9	78.8
	LFDT-Fusion	98.5	89.9	74.0	71.9	64.9	74.4	78.9
	Proposed	**98.7**	**90.0**	73.7	**72.6**	**65.6**	75.0	**79.3**

Table 4: IoU(%) values for DeepLabV3+ on MSRS dataset.
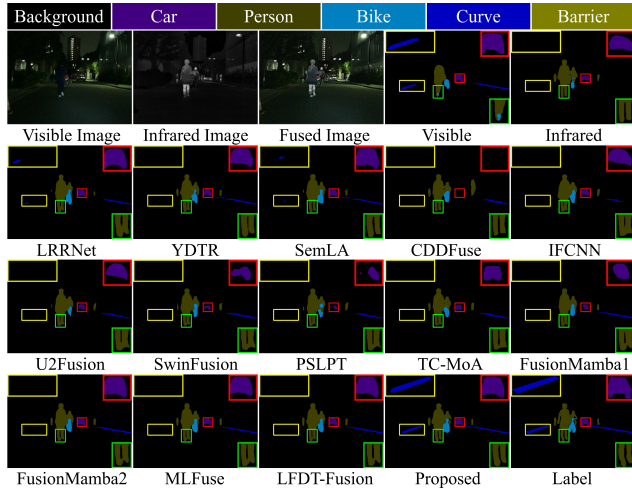

Figure 4: Qualitative segmentation on the MSRS dataset.

Ablation Study

We conduct ablation studies on MSRS for the IVIF task to evaluate each core design, as shown in Table 3. The first part compares Mamba with commonly used operators: convolution layers, window attention, and self-attention. The second part assesses the proposed MAFE and MCCM modules by removing each one to evaluate its individual functionality. The third part evaluate the effectiveness of the feature-level contrastive loss $\mathcal{L}_{fcl}$, the pixel-level contrastive loss $\mathcal{L}_{pcl}$, the workload balancing loss $\mathcal{L}_{wb}$, the expert diversity loss $\mathcal{L}_{div}$, the consensus Loss $\mathcal{L}_{cons}$, and the MCCM loss $\mathcal{L}_{mccm}$. The fourth part validates the effectiveness of the scanning schemes, including spatial-channel scanning, frequency-rotational scanning, and cross-modal scanning. The fifth part examines the scanning directions, comparing single-directional scanning with bidirectional scanning.

Downstream Tasks

To investigate the benefits for downstream visual tasks, we present semantic segmentation results in Table 4. We employ the DeepLabV3+ (Chen et al. 2018) to evaluate performance on the MSRS dataset. Our method achieves the highest mIoU value, demonstrating superior pixel-level segmentation accuracy. As shown in Figure 4, our method produces the most accurate foot and car shapes and is the only one to correctly segment the roadside area.

Conclusions

In this paper, we introduce SMC-Mamba, a Self-supervised Multiplex Consensus Mamba for general image fusion. The MCCM module promotes diverse feature preferences and fusion strategies across experts and enables activated experts to converge toward a unified representation, thereby providing reliable results for image fusion and downstream tasks. The BSCL enhances the preservation of high-frequency details at both feature and pixel levels in a self-supervised manner. The cross-modal scanning captures cross-modal long-range dependencies, enabling seamless integration of complementary information. Meanwhile, MAFE boosts modality-agnostic features by capturing global context and preserving fine-grained local details. Qualitative and quantitative comparisons with the SOTA methods demonstrate the superiority of our proposed SMC-Mamba method.

Acknowledgments

References

Cai, J.; Gu, S.; and Zhang, L. 2018. Learning a deep single image contrast enhancer from multi-exposure images. *IEEE Transactions on Image Processing*, 27(4): 2049–2062.

Chen, L.-C.; Zhu, Y.; Papandreou, G.; Schroff, F.; and Adam, H. 2018. Encoder-decoder with atrous separable convolution for semantic image segmentation. In *Proceedings of the European Conference on Computer Vision (ECCV)*, 801–818.

Fu, J.; Li, W.; Du, J.; and Huang, Y. 2021. A multi-scale residual pyramid attention network for medical image fusion. *Biomedical Signal Processing and Control*, 66: 102488.

Fuoli, D.; Van Gool, L.; and Timofte, R. 2021. Fourier space losses for efficient perceptual image super-resolution. In *Proceedings of the IEEE/CVF International Conference on Computer Vision*, 2360–2369.

Gu, A.; and Dao, T. 2023. Mamba: Linear-time sequence modeling with selective state spaces. *arXiv preprint arXiv:2312.00752*.

Han, D.; Li, L.; Guo, X.; and Ma, J. 2022. Multi-exposure image fusion via deep perceptual enhancement. *Information Fusion*, 79: 248–262.

Hendrycks, D.; and Gimpel, K. 2016. Gaussian error linear units (gelus). *arXiv preprint arXiv:1606.08415*.

Hu, X.; Jiang, J.; Liu, X.; and Ma, J. 2023. ZMFF: Zero-shot multi-focus image fusion. *Information Fusion*, 92: 127–138.

Huang, Q.; Wu, G.; Jiang, Z.; Fan, W.; Xu, B.; and Liu, J. 2024. Leveraging a self-adaptive mean teacher model for semi-supervised multi-exposure image fusion. *Information Fusion*, 102534.

Jordan, M. I.; and Jacobs, R. A. 1994. Hierarchical mixtures of experts and the EM algorithm. *Neural Computation*, 6(2): 181–214.

Lei, J.; Li, J.; Liu, J.; Wang, B.; Zhou, S.; Zhang, Q.; Wei, X.; and Kasabov, N. K. 2025. MLFuse: Multi-Scenario Feature Joint Learning for Multi-Modality Image Fusion. *IEEE Transactions on Multimedia*.

Li, H.; Xu, T.; Wu, X.-J.; Lu, J.; and Kittler, J. 2023. LR-RNet: A novel representation learning guided fusion framework for infrared and visible images. *IEEE Transactions on Pattern Analysis and Machine Intelligence*, 45(9): 11040–11052.

Li, J.; Yu, H.; Chen, J.; Ding, X.; Wang, J.; Liu, J.; Zou, B.; and Ma, H. 2025a. A^2RNet: Adversarial Attack Resilient Network for Robust Infrared and Visible Image Fusion. In *Proceedings of the AAAI Conference on Artificial Intelligence*, volume 39, 4770–4778.

Li, X.; Li, X.; Tan, T.; Li, H.; and Ye, T. 2025b. UMC-Fuse: A Unified Multiple Complex Scenes Infrared and Visible Image Fusion Framework. *IEEE Transactions on Image Processing*.

Liu, J.; Fan, X.; Huang, Z.; Wu, G.; Liu, R.; Zhong, W.; and Luo, Z. 2022a. Target-aware dual adversarial learning and a multi-scenario multi-modality benchmark to fuse infrared and visible for object detection. In *Proceedings of the IEEE/CVF Conference on Computer Vision and Pattern Recognition*, 5802–5811.

Liu, J.; Li, X.; Wang, Z.; Jiang, Z.; Zhong, W.; Fan, W.; and Xu, B. 2024a. PromptFusion: Harmonized semantic prompt learning for infrared and visible image fusion. *IEEE/CAA Journal of Automatica Sinica*.

Liu, J.; Shang, J.; Liu, R.; and Fan, X. 2022b. Attention-Guided Global-Local Adversarial Learning for Detail-Preserving Multi-Exposure Image Fusion. *IEEE Transactions on Circuits and Systems for Video Technology*, 32(8): 5026–5040.

Liu, J.; Wu, G.; Liu, Z.; Wang, D.; Jiang, Z.; Ma, L.; Zhong, W.; and Fan, X. 2024b. Infrared and visible image fusion: From data compatibility to task adaption. *IEEE Transactions on Pattern Analysis and Machine Intelligence*.

Ma, J.; Tang, L.; Fan, F.; Huang, J.; Mei, X.; and Ma, Y. 2022. SwinFusion: Cross-domain long-range learning for general image fusion via swin transformer. *IEEE/CAA Journal of Automatica Sinica*, 9(7): 1200–1217.

Mu, P.; Du, Z.; Liu, J.; and Bai, C. 2023. Little Strokes Fell Great Oaks: Boosting the Hierarchical Features for Multi-exposure Image Fusion. In *Proceedings of the 31st ACM International Conference on Multimedia*, 2985–2993.

Mu, P.; Wu, G.; Liu, J.; Zhang, Y.; Fan, X.; and Liu, R. 2024. Learning to Search a Lightweight Generalized Network for Medical Image Fusion. *IEEE Transactions on Circuits and Systems for Video Technology*, 34(7): 5921–5934.

Nejati, M.; Samavi, S.; and Shirani, S. 2015. Multi-focus image fusion using dictionary-based sparse representation. *Information Fusion*, 25: 72–84.

Peng, S.; Zhu, X.; Deng, H.; Deng, L.-J.; and Lei, Z. 2024. Fusionmamba: Efficient remote sensing image fusion with state space model. *IEEE Transactions on Geoscience and Remote Sensing*.

Rahaman, N.; Baratin, A.; Arpit, D.; Draxler, F.; Lin, M.; Hamprecht, F.; Bengio, Y.; and Courville, A. 2019. On the spectral bias of neural networks. In *International Conference on Machine Learning*, 5301–5310. PMLR.

Sweldens, W. 1998. The lifting scheme: A construction of second generation wavelets. *SIAM Journal on Mathematical Analysis*, 29(2): 511–546.

Tang, L.; Yuan, J.; Zhang, H.; Jiang, X.; and Ma, J. 2022. PIAFusion: A progressive infrared and visible image fusion network based on illumination aware. *Information Fusion*, 83: 79–92.

Tang, W.; He, F.; and Liu, Y. 2023. YDTR: Infrared and Visible Image Fusion via Y-shape Dynamic Transformer. *IEEE Transactions on Multimedia*, 25: 5413–5428.

Wang, W.; Deng, L.-J.; and Vivone, G. 2024. A general image fusion framework using multi-task semi-supervised learning. *Information Fusion*, 102414.

Wang, Y.; Lin, Y.; Meng, G.; Fu, Z.; Dong, Y.; Fan, L.; Yu, H.; Ding, X.; and Huang, Y. 2023. Learning high-frequency feature enhancement and alignment for pan-sharpening. In *Proceedings of the 31st ACM International Conference on Multimedia*, 358–367.

Wang, Z.; Bovik, A. C.; Sheikh, H. R.; and Simoncelli, E. P. 2004. Image quality assessment: from error visibility to structural similarity. *IEEE transactions on image processing*, 13(4): 600–612.

Xiao, G.; Tang, Z.; Guo, H.; Yu, J.; and Shen, H. T. 2024. FAFusion: Learning for Infrared and Visible Image Fusion via Frequency Awareness. *IEEE Transactions on Instrumentation and Measurement*, 73: 1–11.

Xie, H.; Zhang, Y.; Qiu, J.; Zhai, X.; Liu, X.; Yang, Y.; Zhao, S.; Luo, Y.; and Zhong, J. 2023. Semantics lead all: Towards unified image registration and fusion from a semantic perspective. *Information Fusion*, 101835.

Xie, X.; Cui, Y.; Tan, T.; Zheng, X.; and Yu, Z. 2024. Fusionmamba: Dynamic feature enhancement for multimodal image fusion with mamba. *Visual Intelligence*, 2(1): 37.

Xu, H.; Fan, F.; Zhang, H.; Le, Z.; and Huang, J. 2020a. A deep model for multi-focus image fusion based on gradients and connected regions. *IEEE Access*, 8: 26316–26327.

Xu, H.; and Ma, J. 2021. EMFusion: An unsupervised enhanced medical image fusion network. *Information Fusion*, 76: 177–186.

Xu, H.; Ma, J.; Jiang, J.; Guo, X.; and Ling, H. 2020b. U2Fusion: A unified unsupervised image fusion network. *IEEE Transactions on Pattern Analysis and Machine Intelligence*, 44(1): 502–518.

Xu, H.; Ma, J.; Le, Z.; Jiang, J.; and Guo, X. 2020c. Fusiondn: A unified densely connected network for image fusion. In *AAAI Conference on Artificial Intelligence*, volume 34, 12484–12491.

Xu, Z.-Q. J. 2020. Frequency Principle: Fourier Analysis Sheds Light on Deep Neural Networks. *Communications in Computational Physics*, 28(5): 1746–1767.

Yang, B.; Jiang, Z.; Pan, D.; Yu, H.; Gui, G.; and Gui, W. 2025. LFDT-Fusion: a latent feature-guided diffusion Transformer model for general image fusion. *Information Fusion*, 113: 102639.

Zhang, H.; Cao, L.; Zuo, X.; Shao, Z.; and Ma, J. 2025. OmniFuse: Composite degradation-robust image fusion with language-driven semantics. *IEEE Transactions on Pattern Analysis and Machine Intelligence*, 47(9): 7577–7595.

Zhang, H.; Le, Z.; Shao, Z.; Xu, H.; and Ma, J. 2021. MFF-GAN: An unsupervised generative adversarial network with adaptive and gradient joint constraints for multi-focus image fusion. *Information Fusion*, 66: 40–53.

Zhang, X. 2021. Benchmarking and comparing multi-exposure image fusion algorithms. *Information Fusion*, 74: 111–131.

Zhang, Y.; Liu, Y.; Sun, P.; Yan, H.; Zhao, X.; and Zhang, L. 2020. IFCNN: A general image fusion framework based on convolutional neural network. *Information Fusion*, 54: 99–118.

Zhao, Y.; Zheng, Q.; Zhu, P.; Zhang, X.; and Ma, W. 2023a. TUFusion: A transformer-based universal fusion algorithm for multimodal images. *IEEE Transactions on Circuits and Systems for Video Technology*.

Zhao, Z.; Bai, H.; Zhang, J.; Zhang, Y.; Xu, S.; Lin, Z.; Timofte, R.; and Van Gool, L. 2023b. Cddfuse: Correlation-driven dual-branch feature decomposition for multi-modality image fusion. In *Proceedings of the IEEE/CVF Conference on Computer Vision and Pattern Recognition*, 5906–5916.

Zhu, L.; Liao, B.; Zhang, Q.; Wang, X.; Liu, W.; and Wang, X. 2024a. Vision mamba: Efficient visual representation learning with bidirectional state space model. *arXiv preprint arXiv:2401.09417*.

Zhu, P.; Sun, Y.; Cao, B.; and Hu, Q. 2024b. Task-customized mixture of adapters for general image fusion. In *Proceedings of the IEEE/CVF Conference on Computer Vision and Pattern Recognition*, 7099–7108.